Supplementary Information (SI) for Journal of Materials Chemistry B.

Cu-doped Co_9S_{8-x} sonozymes for enhanced sonodynamic and chemodynamic therapy of gallbladder cancer through ion doping and vacancy engineering

Qingxiang Gao[a,1], Xi Yang[b,1], Ni An[c,1], Yang Shen[a], Weilai Ji[d], Lei Wang[e], Kaijian Chu[a], Chengjian He[f,*], Qing Ouyang[g,*], Zhilin Sha[a,*]

[a] Department I of Biliary Tract Surgery, Eastern Hepatobiliary Surgery Hospital, Naval Medical University, Shanghai 201823, China

[b] Department of General Surgery, The Affiliated Shuyang Hospital of Xuzhou Medical University, Suqian, Jiangsu 223600, China

[c] Department of Anesthesiology, The Eighth medical center of Chinese PLA General Hospital, Beijing 100091, China

[d] Department of Hepatobiliary Surgery and Liver Transplant Center, Shenyang 4th hospital, Shengyang, Liaoning 110031, China

[e] Department of General Surgery, Yancheng Hospital of Traditional Chinese Medicine, Yancheng, Jiangsu 201823, China

[f] Department of Mini-invasive Intervention Center, Eastern Hepatobiliary Surgery Hospital, Naval Medical University, Shanghai 201823, China

[g] Department of Hepatobiliary Surgery and Liver Transplant Center, PLA General Hospital of Southern Theatre Command: People's Liberation Army General Hospital of Southern Theatre Command, Guangzhou, Guangdong 510010, China

* Corresponding author.

E-mail address: chengjianhesjtu@163.com (C. He); kanshine@163.com (Q. Ouyang); szl_dr@qq.com (Z. Sha)

[1] These authors contributed equally to this work.

Keywords: Co_9S_{8-x}, ion doping engineering, vacancy engineering, sonodynamic therapy, chemodynamic therapy

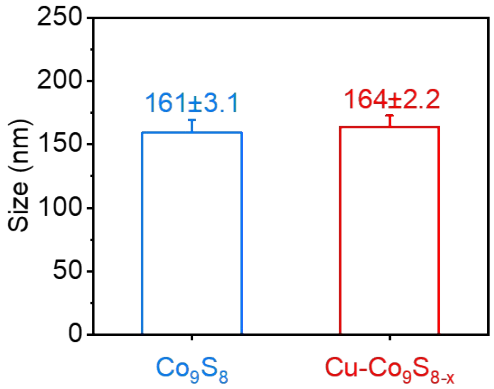

Fig. S1. DLS size of Co_9S_8 and Cu-Co_9S_{8-x}. Data are presented as the mean ± SD. (n = 3).

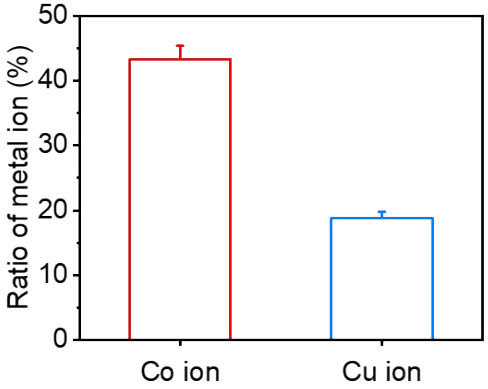

Fig. S2. The contents of Co and Cu ions in Cu-Co_9S_{8-x} determined by ICP-MS Data are presented as the mean ± SD. (n = 3).

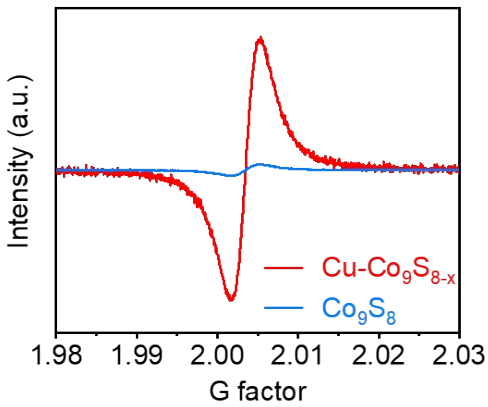

Fig. S3. EPR spectrum of Co_9S_8 and Cu-Co_9S_{8-x}.

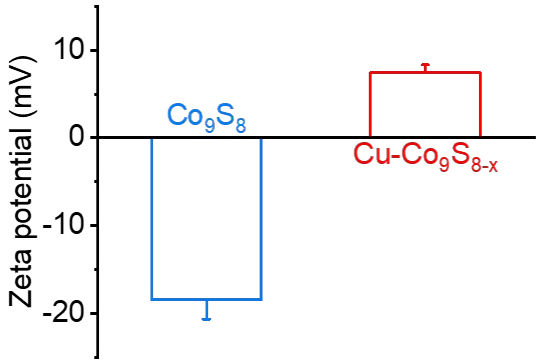

Fig. S4. Zeta potential of Co_9S_8 and Cu-Co_9S_{8-x}. Data are presented as the mean ± SD. (n = 3).

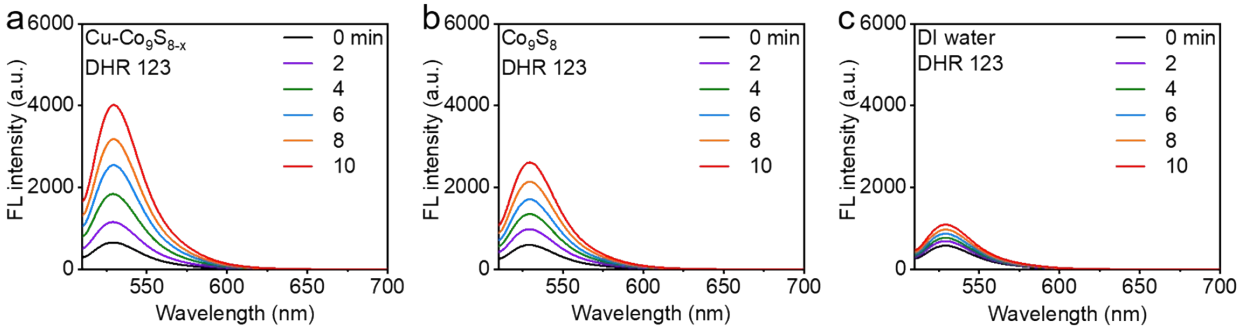

Fig. S5. Measurement of the $O_2^{-\bullet}$ generation of Cu-Co_9S_{8-x} and Co_9S_{8-x} under US irradiation (50 kHz, 1.0 W/cm^2).

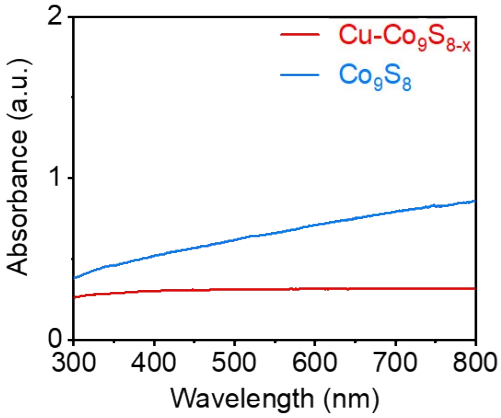

Fig. S6. UV-vis absorption of Co_9S_8 and Cu-Co_9S_{8-x}.

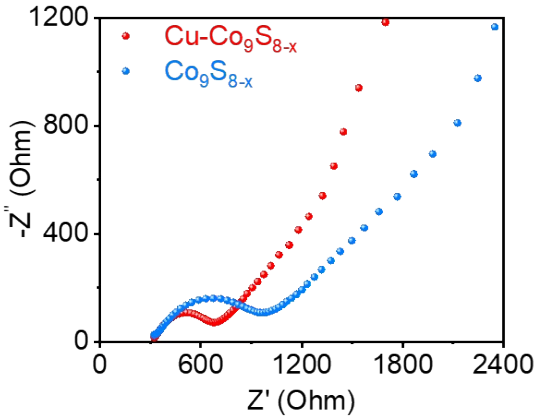

Fig. S7. The impedance spectra of Co_9S_{8-x} and Cu-Co_9S_{8-x} electrodes.

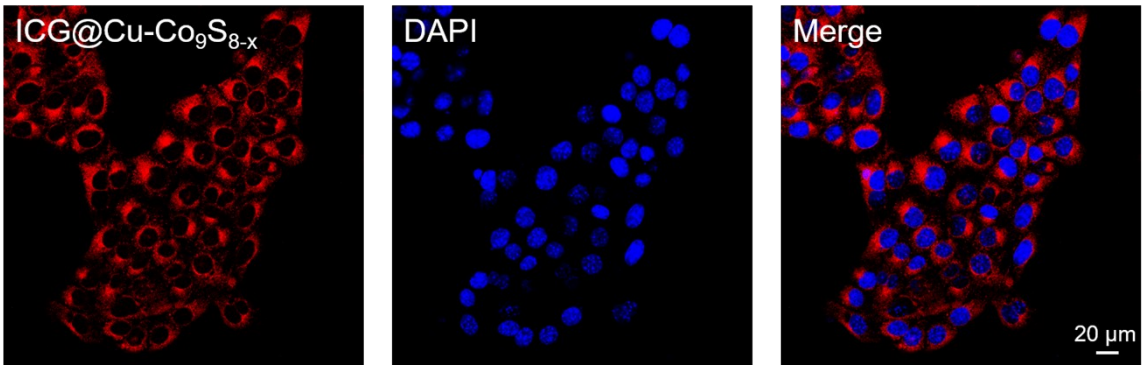

Fig. S8. Confocal images of NOZ cells after being treated with ICG-labeled Cu-Co_9S_{8-x} and DAPI.

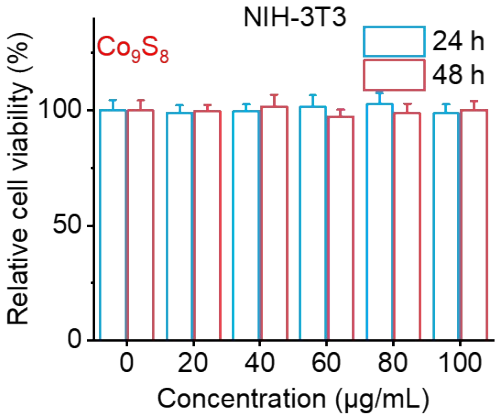

Fig. S9. Relative cell viabilities of NIH-3T3 cells incubated with Co_9S_8 with varied concentrations for 24 or 48 h. Data are presented as the mean ± SD. (n = 6).

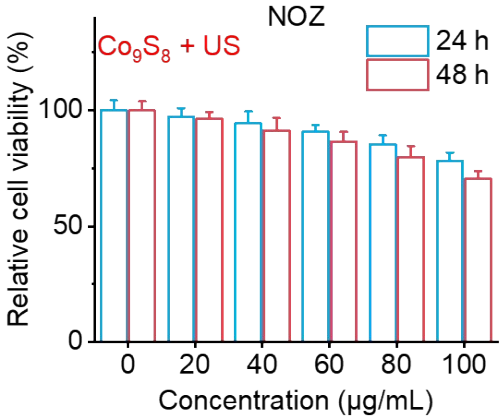

Fig. S10. Relative cell viabilities of NOZ cells incubated with Co_9S_8 with varied concentrations for 24 or 48 h under US irradiation. Data are presented as the mean ± SD. (n = 6)

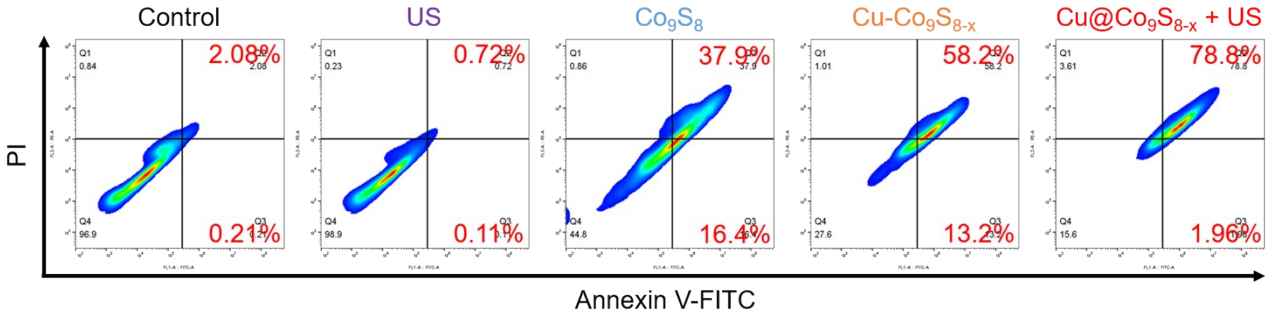

Fig. S11. Apoptosis assay of NOZ cells after different treatments through flow cytometry.

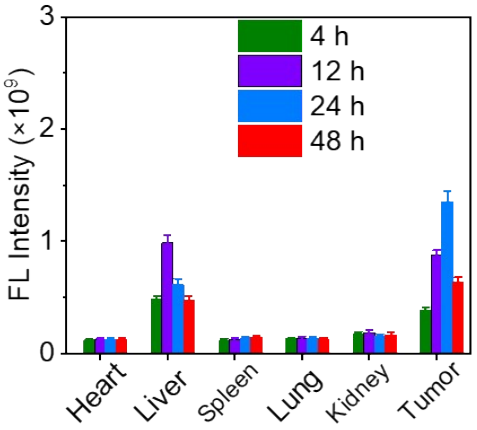

Fig. S12. Time-dependent fluorescence intensity of Cu-Co_9S_{8-x} in the major organs and tumor tissues. Data are presented as the mean ± SD. (n = 5).

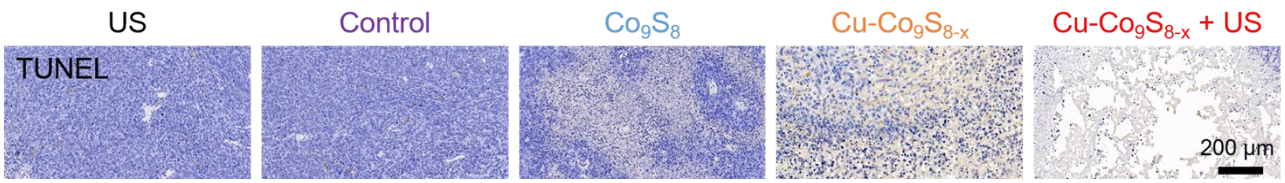

Fig. S13. TUNEL staining of tumors in mice after different treatments.

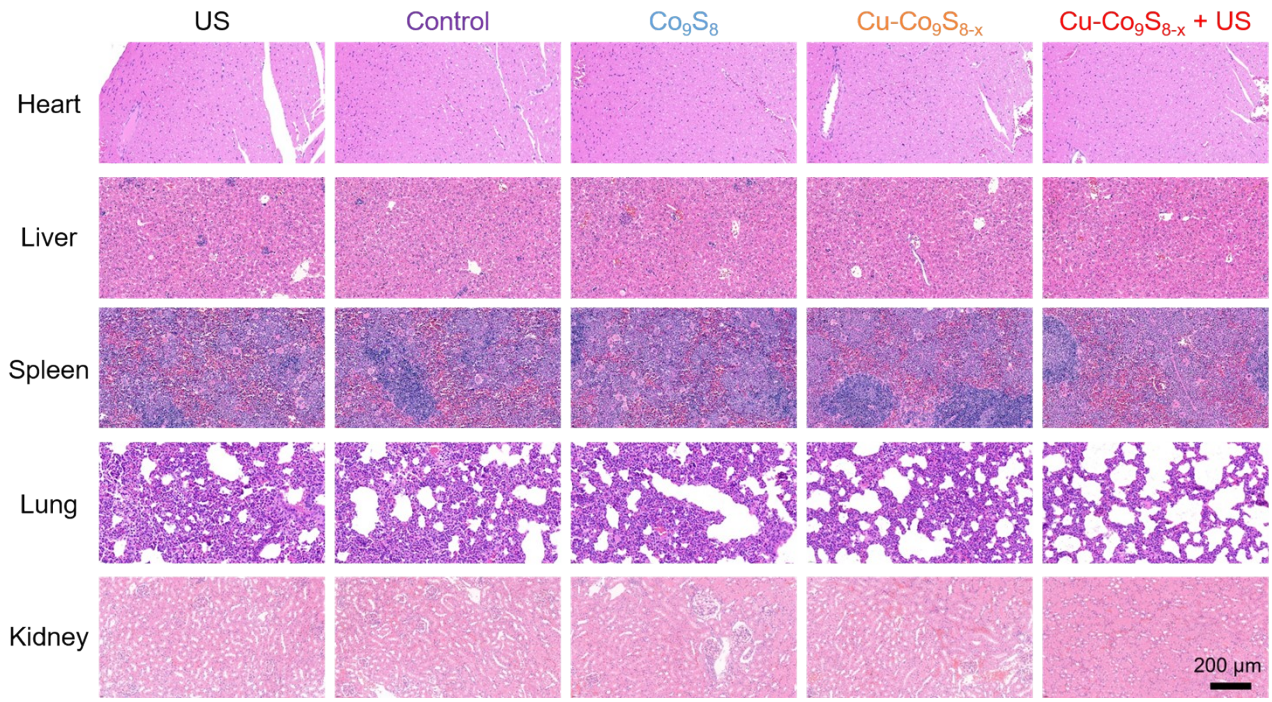

Fig. S14. H&E-stained images obtained from the major organs (heart, liver, spleen, lung, and kidney) of mice in different treatment groups.

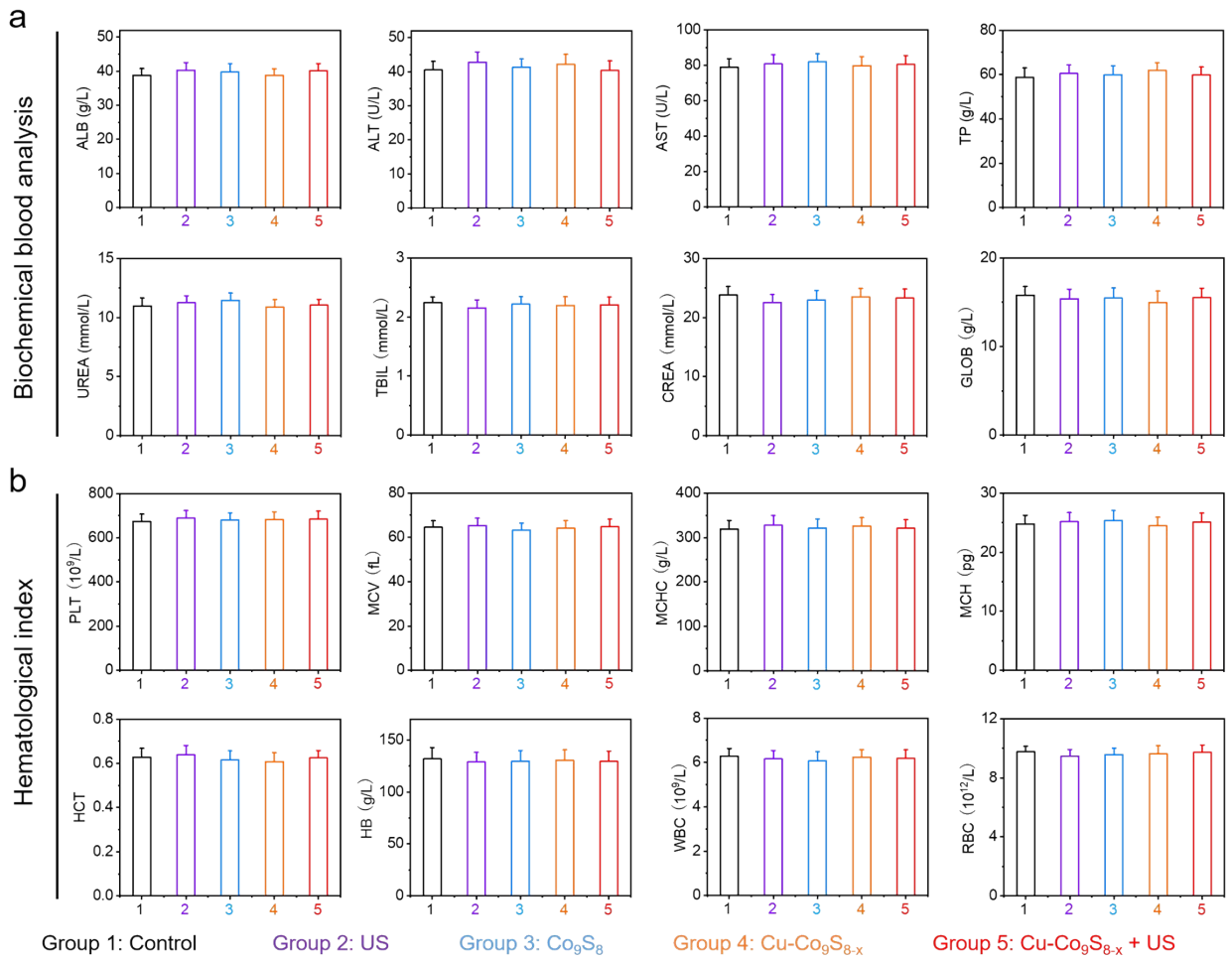

Fig. S15. (a-b) Biochemical blood analysis (a) and hematological index (b) of the mice that were sacrificed 18 days after different treatments.